

EFFECT OF THUMB ABDUCTION AND **ADDUCTION** ON **HYDRODYAMIC** CHARACTERISTICS OF A MODEL OF THE HUMAN HAND

Hideki Takagi ¹, Yukimaru **Shimizu** ², **Akihiro** Kurashima ², Ross Sanders ³

1: Faculty of Education, 2: Faculty of Engineering,

Mie University, 1515 kamihama, Tsu, Mie, , JAPAN

3: Dept. Physical Education Sport and Leisure Studies,
The University of Edinburgh, Edinburgh, UK

The purpose of this study was to compare hydrodynamic characteristics of human hand models with the thumb abducted and the thumb adducted using pressure differential and flow visualization techniques. Two different models of an adult man's right hand (Model A, the hand with abducted thumb; Model B, the hand with thumb adducted) were made with polyester resin. The magnitudes of pressure acting on holes located at the hand model surfaces were measured for various pitch angles to a flow of air in a wind tunnel. Flow visualization of air around the model was conducted using a laser beam. By means of the pressure data, the magnitudes of fluid force were calculated. The experimental results revealed that the thumb position has a large influence on the pressure distribution. The difference of the pressure distribution affected the hydrodynamic characteristics.

KEYWORDS: Sports engineering, swimming, pressure distribution, flow visualization, hydrodynamic characteristics, human hand model

INTRODUCTION: Hydrodynamic characteristics of a human hand have been discussed in several studies (e.g. Schleihauf, 1979, Berger et al., 1995, Sanders, 1999). Schleihauf has determined lift and drag coefficients under conditions in which velocity was constant. These coefficients were used together with digitized three-dimensional data of the hand to estimate the lift, drag, and resultant force vectors produced during the stroke. Berger et al. have extended Schleihau's work by estimating the contribution of the hand alone and the combine forearm and hand by varying the immersion depth of the model. Sanders' experiments included acceleration of the hand to obtain additional coefficients enabling forces acting on an accelerating hand to be estimated. Berger et al. (1997) found that models with different thumb abduction/adduction and finger spread had very little effect on drag forces but had an effect on lift forces. Sanders (personal communication) found that thumb adduction increased drag forces but that this was offset by a reduction in hand cross sectional area. Slight differences in the pattern of lift and drag coefficients across angles of hand orientation to the flow were also found.

However, there remains much to be learned about the effect of thumb abduction/adduction and whether similar results are obtained by different methods of testing. If a swimmer knows the effect of abducting or adducting the thumb then their technique may be modified to optimize propulsion and reduce drag. Takagi and Wilson (1999) pioneered a method whereby drag and lift forces acting on the hand can be estimated from direct measurement of pressure differences between the front and back of the hand. Supplementing pressure data with observation of the flow using flow visualization techniques may improve understanding of differences in drag and lift across hand orientations to the flow and shape differences due to variation in thumb position. Therefore, the purpose of this study was to compare hydrodynamic characteristics of human hand models with the thumb abducted and the thumb adducted using pressure differential and flow visualization techniques.

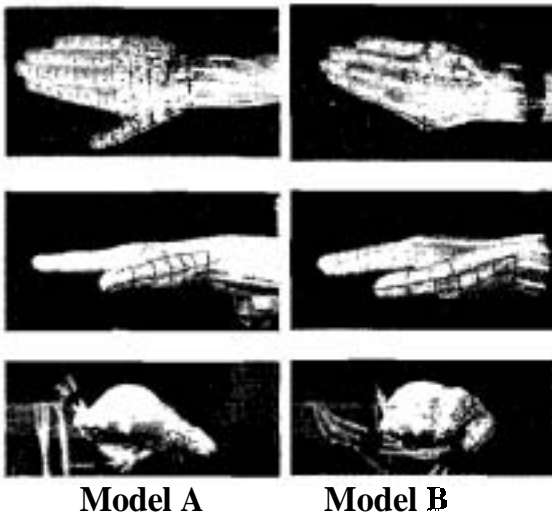


Figure 1 - Two types of human hand (Model A, the hand with abducted thumb; Model B, the hand with thumb adducted)

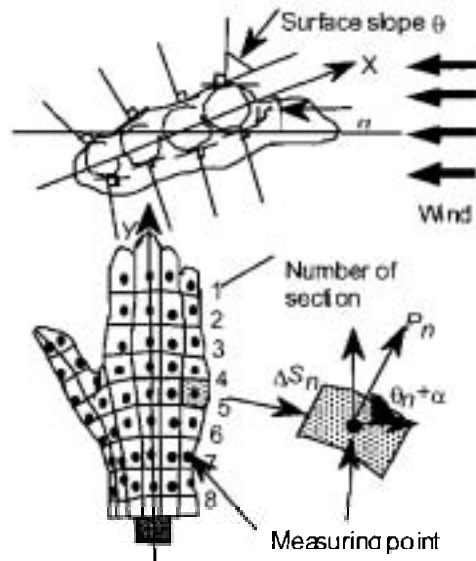


Figure 2 - Definitions of hand orientation and procedures for calculating lift and drag for each hand division.

METHOD: Two different models of an adult man's right hand were made with polyester resin (Figure 1). Both models had the fingers together. The thumb was abducted in Model A, and adducted in Model B. The hand model was fixed in the center of the wind tunnel. To measure pressure, grooves were cut in the palm and the back of the model, and pipes were inserted in the grooves. Several small holes (diameter 1 mm) were then made vertically to the surface of each pipe. A pressure sensor was connected to each pipe through a scani-valve. When the pressure was measured, only one hole was left open for each pipe, and the other holes were covered with vinyl tape. The pressure data were digitized after amplification and input to a personal computer (sampling frequency 240 Hz). The flow velocity was set at 12 m/s. The Reynolds number equaled 2.72×10^5 at 0.8 m/s in fresh water at 26 degrees Celsius.

A definition of angles and a procedure for analyzing the pressure data are shown in Figure 2. There were a total of 88 measuring points on the surface of the model. We defined a line passing through the metacarpophalangeal II to metacarpophalangeal V joints as the X axis, and a perpendicular line, which went through the middle finger as the Y axis. The angle of attack (α) was defined as the angle between the X axis and the wind flow vector projected onto the hand plane, and varied from zero to 180 degrees in 5 degree increments. When α is between zero to 90, the thumb leads, and when α is from 90 to 180, the little finger leads. The sweepback angle was defined as the angle between the Y axis and the wind flow vector projected onto the hand plane. Although the experiment was conducted to vary the sweep-back angle, only data under conditions in which the sweep-back angle equaled zero, are presented in this paper. The hand's surface was divided into 88 sections at each measuring point, and measured its area respectively. The pressure measured at the particular point in the center of each division was deemed to represent the pressure over that division. The pressure values were transformed into the coefficient of pressure (C_p) by the following formula,

$$C_p = (P_n - P_{air}) / 0.5 \rho U^2 \quad (1)$$

Where P_n represents real pressure value, P_{air} represents atmospheric pressure, ρ represents density of air. This formula comes from the well known formula $C_D = F_D / 0.5 \rho S U^2$.

As the pressure (P_n) acts normal to the surface, and assuming that the surface is a plane, lift and drag components may be estimated. The pressure having a lift effect was obtained as the sine of the pressure (P_n) and the pressure having a drag effect as the cosine of the pressure (P_n). For each division, the lift and drag force were determined by multiplying these respective

pressure effects by the area of the division. Finally, entire lift force (L) and drag force (D) acting on the hand were obtained by integrating over the whole hand surface.

$$L = \sum_{n=1}^{88} \Delta S_n P_n \text{Sin}(\theta_n + \alpha) \quad (2)$$

$$D = \sum_{n=1}^{88} \Delta S_n P_n \text{Cos}(\theta_n + \alpha) \quad (3)$$

Where S_n is the area of the division n , and P_n is the real pressure value measured at the center of the division n . The lift and drag force values were transformed into the coefficients of lift and drag (C_L , C_D) by the following formula,

$$C_L = L / 0.5 \rho S U^2 \quad (4)$$

$$C_D = D / 0.5 \rho S U^2 \quad (5)$$

Where S is total hand plane area.

Flow visualization of air around the model was conducted using an argon laser beam and smoke injected into the flow by a smoke generator. The flow velocity was set at 4 m/s, and the laser beam irradiated along each cross-section as shown in Figure 2. The streams of smoke were recorded from the side by a digital video camera and the images were processed digitally to yield pictures of the flow.

RESULTS AND DISCUSSION: The hand's lift-drag characteristics of the two models are compared in Figure 3. A vertically upward direction against the flow vector was set as positive referring to the coefficient of lift. Between the two models, Model A showed higher lift coefficients than Model B in a thumb-leading orientation, that is at α angles of between 0-90 degrees. In particular, Model A indicated positive lift values but Model B indicated negative lift values in the relatively low α angles. While in a little finger-leading orientation, that is at α angles of between 90-180 degrees, Model B generated greater lift than Model A. As concerns the drag coefficient, Model B showed relatively higher values than Model A in a little finger-leading orientation.

Figure 4 shows the pressure distribution for different sections of the two models. The flow visualization pictures corresponding to Figure 4 are shown in Figure 5. These show the pressure distribution and the flow patterns for two conditions, which were effective in generating lift force in each model (Model A, $\alpha=50$; Model B $\alpha=150$). For comparison, two standard conditions (i.e. Model A, $\alpha=0$; Model B, $\alpha=180$) are also shown. In Figure 4(a) and 5(a) the lift coefficient reached the highest value among all experimental conditions because the palm side value (■)

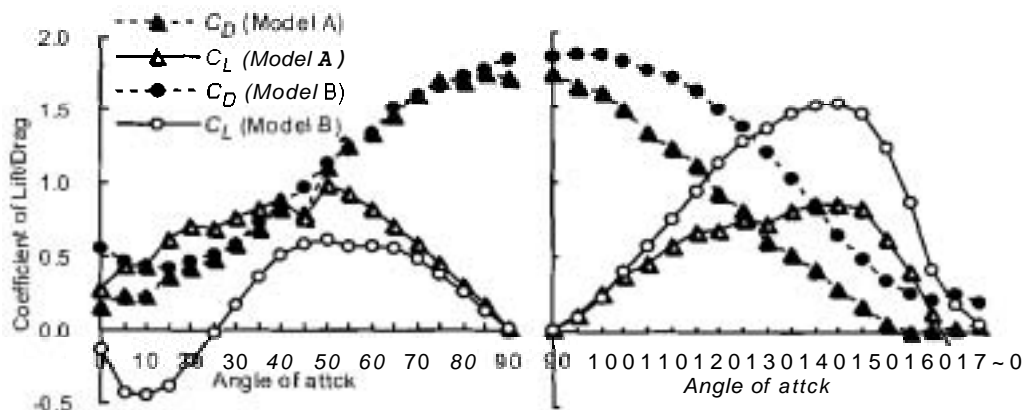


Figure 3 - The coefficient of drag and lift of the two models plotted against the angle of attack. Left part: a thumb-leading orientation, right part: a little finger-leading orientation.

was increased and the back side value (●) was decreased. This large pressure differential was due to the flow on the back side flowing rapidly along the surface so that the pressure value became negative. On the other side, the flow collided against the palm and pushed the hand downward, this pressure was higher than the atmospheric pressure. Compared to the condition when $\alpha=150$, a relatively small pressure differential was observed when $\alpha=180$ in Model B. The flow was almost symmetrical with respect to the X-axis but the pressure distributions were very complicated. As a result, the coefficient of lift was nearly zero, because the negative pressure differential at the leading edge was balanced with the positive one at tail edge.

When the thumb became the leading edge, the highest lift coefficient was observed at $\alpha=50$ in Model A. According to Figure 4(c), 5(c), a downdraft on the palm occurred but the separation of flow at the middle of the backside was also observed, the pressure differential was not increased as much as Model B at $\alpha=150$. When $\alpha=0$ in Model A, the only positive pressure was observed at leading edge of thumb, while all other locations had negative pressure. Thus, the pressure differential was small, and the coefficient of lift became nearly zero.

CONCLUSION: The experimental results revealed that adduction and abduction of the thumb influence the fluid force over the entire hand. In particular, there was a difference in generating the lift force. When the thumb side became a leading edge, the model with the abducted thumb. Model A, seems to be advantageous for generating lift force. When the little finger leads, the Model B, an adducted thumb can produce more lift force. According to an analysis of the pressure distribution, it was clarified that this lift force was caused by a pressure increase on the palm and a pressure decrease on the back of the hand. Moreover, by flow visualization an effect of thumb adduction on the flow was confirmed directly. Since each swimmer has a different hand shape it seems unwise to generalize the results. However, there are indications that thumb position may play an important role in optimizing swimming technique.

REFERENCES:

- Berger, M.A.M., Groot, G.de. & Hollander, A.P. (1995). Hydrodynamic drag and lift forces on human hand/arm models. *Journal of Biomechanics*, **28**, 125-133.
- Berger, M.A.M. Groot, G.de. & Hollander, A.P. (1997). Influence of hand shape on force generation during swimming. In B.O. Eriksson & L. Gullstrand (Eds.) *Proceedings of the XII FINA Congress on Sports Medicine* (pp.389-396). Goteborg: Federation Internationale De Natation Amateur.
- Sanders, R.H. (1999). Hydrodynamic characteristics of a swimmer's hand. *Journal of Applied Biomechanics*, **15**, 3-26.
- Sanders, R.H. Effect of Thumb Abduction of Drag and Lift Coefficients of a Swimmer's Hand. Personal communication – in preparation for publication.
- Schleihauf, R.E. (1979). *A Hydrodynamic Analysis of Swimming Propulsion*. Swimming 111 (pp.173-184). Baltimore: University Park Press.
- Takagi, H. & Wilson, B. (1999). Calculating hydrodynamic force by using pressure differences in swimming. *Biomechanics and Medicine in Swimming VIII* (pp.101-106). Jyvaskyla: Gummerus Printing.

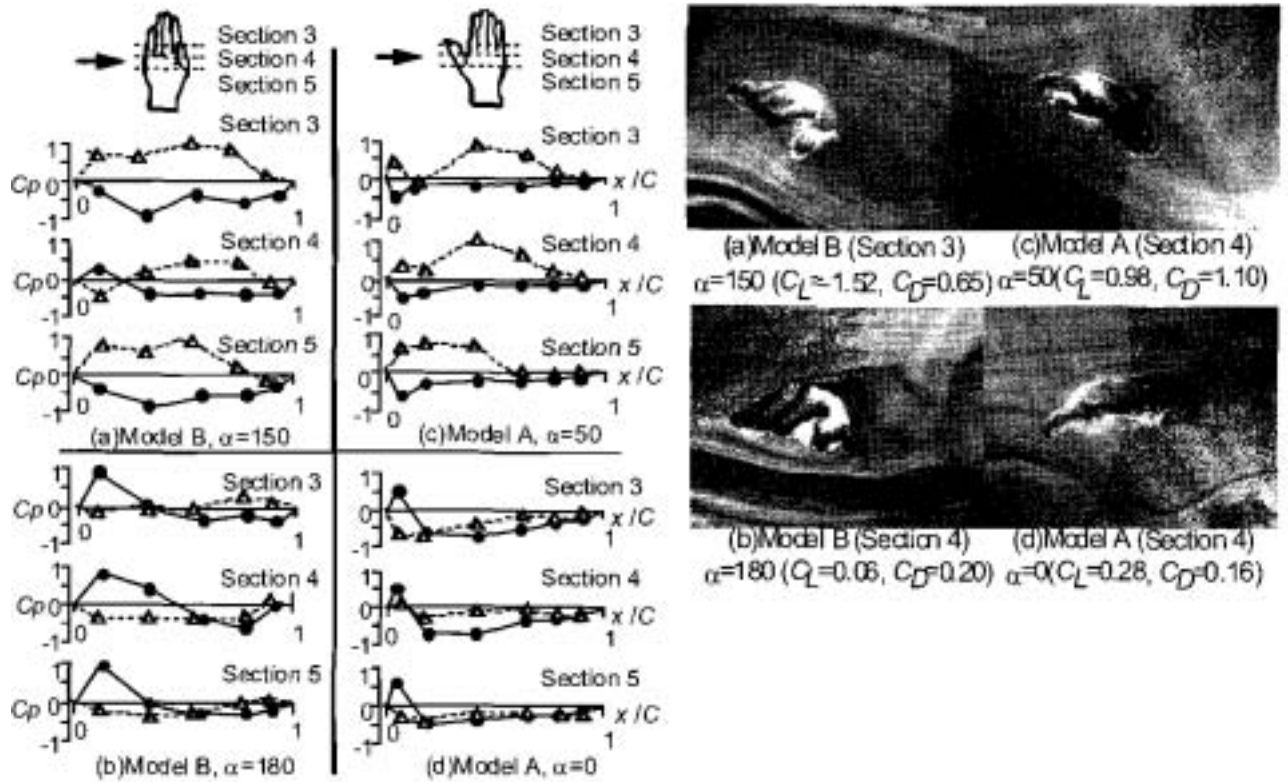


Figure 4 - (Left) Pressure distribution on the cross-section 3, 4, 5 of (be hand model. The x-axis indicates the relative measurement position (x) when the chord length of the section (C) equals 1. The y-axis indicates the coefficient of pressure. (:pəɪnɪ, :back)

Figure 5 - (Right) Flow visualizations of air around the hand models at the particular section related to the pressure distribution figures.